Curr Radiol Rep (2017) 5:35
DOI 10.1007/s40134-017-0226-8

Dual-Energy CT in Focal and Diffuse Liver Disease

Anushri Parakh[1] · Vinit Baliyan[1] · Dushyant V. Sahani[1]

Published online: 27 May 2017

Abstract
Purpose of Review The purpose of this article is to review recent literature evaluating the role of dual-energy CT (DECT) in assessing focal and diffuse liver diseases.
Recent Findings Recent generation of DECT scanners and newer DECT technologies are equipped with advanced multi-material decomposition algorithms and have better spectral separation capabilities. These have the potential for improvement in quantitative assessment of deposition disorders. Advancements in image reconstructions have also demonstrated enhanced detection hypovascular and hypervascular liver lesions.
Summary This article will provide an updated overview of a wide array of clinical applications of DECT in liver imaging with case illustrations.

Keywords Dual-energy computed tomography · Spectral CT · Liver disease · Hepatic applications · Material-specific iodine

This article is part of the Topical collection on *Dual Energy CT*.

✉ Dushyant V. Sahani
dsahani@mgh.harvard.edu

Anushri Parakh
aparakh1@mgh.harvard.edu

Vinit Baliyan
vbaliyan@mgh.harvard.edu

[1] Division of Abdominal Imaging, Department of Radiology, Massachusetts General Hospital, White 270, 55 Fruit Street, Boston, MA 02114, USA

Introduction

CT data acquisition is based on X-ray production by decelerating electrons which are passed through a patient and then illuminate detectors. X-rays are polychromatic in nature with a wide range of spectral data. In dual-energy CT (DECT), this poly-spectral nature of X-rays along with the principle of photoelectric effect is exploited to obtain material-specific attenuation information. DECT has garnered a lot of interest in abdominal imaging and has a role in diagnosis and management of focal and diffuse liver diseases [1, 2]. A recent consensus statement by the Society of Computed Body Tomography and Magnetic Resonance (SCBT-MR) has stated that liver DECT imaging is valuable for quantitative assessment of diffuse liver diseases such as fatty liver or iron storage diseases, contrast uptake in focal hepatic lesions, focal treatment ablation sites, and vascular thrombus characterization, especially during serial monitoring [3].

Understanding the utility and challenges of this imaging technology is important for radiologists to incorporate this technique into clinical practice. This review discusses the technical considerations when using DECT for hepatic imaging and provides an overview of recent literature assessing its role in focal and diffuse liver pathologies.

Technical Considerations

Spectral information for DECT can be obtained by a multitude of approaches, depending on the manufacturer. It is commonly acquired by a *source-based* approach using X-ray beams of low (80 or 100 kVp) and high energies (140 or 150 kVp) either on a single-source system (ssDECT; with fast kV switching or split-filter technology)

or on a dual-source system (dsDECT; with two angularly offset tube–detector assembly). It can also be obtained by *detector-based* approach where X-ray of a single potential of 120 kVp (same as SECT) is applied and the differential energy separation occurs at the level of the detector (ssDECT system with layered or photon counting detectors). In this review, ssDECT images are obtained using the fast kV switching approach and dsDECT images are obtained on a second-generation dsDECT scanner [4•].

Awareness of each technique's strengths and limitations is important before investment and inculcation into clinical routine. For example, fast-switching ssDECT technique provides a larger effective dual-energy field of view (DE-FOV; 50 cm), but there is no tube current modulation. In contrast, while tube current modulation is possible in dsDECT, the DE-FOV is limited, particularly in earlier generations. Due to a limited DE-FOV centering of patient within the gantry according to the organ of interest, in this case the liver becomes critical. Fink et al. suggested the use of a thick collimation and centering the patient to the left in the first-generation dsDECT to compensate for the restricted FOV (26 cm) [5, 6]. Second- and third-generation dsDECT scanners have a tin filter at the high-energy tube output allowing for better spectral separation. These scanners also provide a larger DE-FOV and better spatial resolution due to the use of thinner collimation.

The contrast injection protocols for DECT liver imaging are not different than in conventional SECT [6]. Patient history governs the choice of contrast phase for DECT acquisition, arterial, portovenous, delayed, or a combination of these phases (Table 1). Table 2 describes the DECT protocols used in our institution, when a hypervascular liver lesion is suspected.

Image Reconstructions

For hepatic applications, DECT datasets are post-processed to yield (a) blended images (unique to dsDECT), (b) virtual monochromatic images, and (c) material-specific images, including virtual unenhanced (VUE) images.

It is important to produce datasets that possess image characteristics comparable to conventional 120-kVp SECT acquisition. 65-keV images from fast-switching ssDECT systems [7, 8] and a linear blend [9] with equal weightage (0.5) of low- and high-energy data from dsDECT have been shown to possess the optimal contrast-to-noise ratio (CNR) for abdominal interpretation. At our institution, these are sent to PACS for diagnostic interpretation in all three planes. Virtual *monochromatic* or *monoenergetic* (VME) images at various levels of photon energy (40–190 keV) are not used for routine interpretation due to constraints in interpretation time and data storage. However, several in vitro and in vivo studies have shown that low-energy (50 keV) images improve the lesion delineation and are thus sent to PACS in our institution in axial plane. Depending upon the vendor, *material-specific* images are generated by two-material, three-material, or multi-material decomposition methods [7, 10, 11, 12•]. The most common material pair used for liver is iodine and water. Material-specific iodine (MS-I) images depict the distribution of iodine, quantitatively and qualitatively, throughout the image and 'water' image represents a VUE image. Besides iodine, other materials of interest in liver are fat and iron. This series of images can also be processed as color overlays [13].

Different clinical applications of these image reconstructions for focal and diffuse liver diseases are described below.

Lesion Detection

DECT can improve delineation of both hyper- and hypovascular lesions by accentuating the lesion to liver parenchyma contrast. In low-keV arterial phase images, iodine within the hypervascular lesions shows higher attenuation as compared to the background liver increasing the conspicuity of the lesion (Fig. 1), whereas hypovascular lesions scanned in portovenous phase at low keV show lower attenuation as compared to the parenchyma due to a greater distribution of iodinated contrast within the normal hepatic tissue (Fig. 2). Different DECT techniques have been successfully evaluated for this application and a review of literature is outlined in Table 3 [14–20]. Recently, an in vitro study performed on layer-detector ssDECT also showed higher CNR of both hyper- and hypovascular lesions on low-keV images [21]. Irrespective of lesion and scanner type, the increased CNR at low photon energies reveals more lesions (Fig. 3) with increased acuity and improved definition of margins (Fig. 4). This is especially useful in assessing the extent of diffuse infiltrative masses and surgical planning [22•].

An important limitation with the use of low-energy monochromatic images is higher intrinsic image noise [15]. To overcome increased image noise at low keV in ssDECT, Gao et al. have suggested the use of fused VME images to display both HCC and the surrounding anatomy without compromise [23]. Recent ex vivo and in vivo studies have also evaluated a new post-processing algorithm (advanced VME or VME plus images) on dsDECT, which maintains the noise of high-energy scans while retaining the contrast of low-energy scans in evaluating both hyper- and hypovascular lesions [20, 24•, 25]. These studies have demonstrated improved assessment of liver lesions at low keV with VME plus images, as compared to conventional VME

Table 1 Author recommendations for phase of DECT acquisition

Clinical questions	DECT acquisition phase
Fatty liver, hemochromatosis	Unenhanced
Hypervascular lesions	Arterial phase
Hepatocellular carcinoma	
Metastasis from	
Renal cell carcinoma	
Neuroendocrine tumor	
Melanoma	
Hypovascular lesions	Portovenous phase
Cholangiocarcinoma	
Diffuse or infiltrative mass	
Metastasis from sites (other than above)	
Indeterminate and/or infiltrative mass for lesion characterization	Arterial and portovenous phases
Fibrosis	Delayed phase

Table 2 Protocols for focal liver lesion imaging on three types of scanners with DECT acquisition performed in arterial phase

Parameters	ssDECT	dsDECT (second generation)	dsDECT (third generation)
Tube potential (kVp)	80/140	100/140 Sn	100/150 Sn
Tube current modulation	No	Yes	Yes
Tube current (mA)	Under 150 lbs: 640	Reference 200 mA	Reference 200 mA
	151–250 lbs: 600		
Scanning mode	GSI under 150 lbs: 16	Dual energy	Dual energy
	151–250 lbs: 11		
Detector collimation (mm)	Under 150 lbs: 40 × 0.6	32 × 0.6	40 × 0.6
	151–250 lbs: 40 × 0.8		
FOV (cm)	50	33	35.4
Pitch	1.375	0.95	0.95
Iterative reconstruction	ASIR (50%)	SAFIRE level 3	SAFIRE level 3
Datasets	50 keV	50 keV	50 keV
	65 keV	Blended (0.5)	Blended (0.5)
	VUE images	VUE	VUE
	MS-I images	Iodine color overlay	Iodine color overlay

Fast kV switching ssDECT (Discovery 750 HD, GE Healthcare) and dsDECT (second and third generations, Somatom Definition FLASH and FORCE, respectively, Siemens Healthcare) systems are present in our institution

ssDECT single-source DECT, *dsDECT* dual-source DECT, *Sn* tin filter at the output of high-energy tube, *GSI* gemstone spectral imaging, *ASIR* adaptive statistical iterative reconstruction, *SAFIRE* sinogram-affirmed iterative reconstruction, *VUE* virtual unenhanced images, *MS-I* material-specific iodine images

and blended images without degradation in image quality, but with limitations in large-sized patients. The optimal VME level for hypervascular lesion detection is significantly influenced by patient size and must be taken into consideration while developing clinical protocols [26].

Besides lesion detection, the VME plus dsDECT and fused VME ssDECT images have also been shown to improve CNR of intrahepatic vasculature in comparison to conventional images [27, 28]. This is useful in diagnosing Budd–Chiari syndrome, interventional planning, and in patients with altered hemodynamics secondary to chronic liver diseases.

Mass Characterization

Upon detection, correct characterization of hepatic lesions is crucial. SECT is the standard imaging modality of choice for characterization of most liver lesions. For lesions that

Fig. 1 Improved conspicuity of hypervascular lesion. ssDECT performed in arterial phase on a 63-year-old male with cirrhosis. 50-keV and MS-I image increases the conspicuity of the hypervascular lesion (*arrow*) in segment II, which otherwise appears innocuous on 65-keV SECT-equivalent image. Biopsy of the lesion confirmed the diagnosis of hepatocellular carcinoma

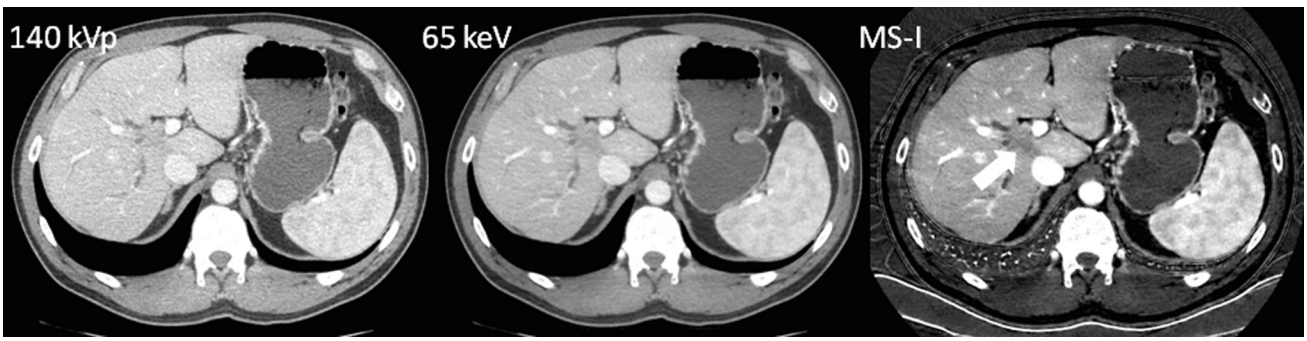

Fig. 2 Improved delineation of hypovascular lesion. ssDECT performed in portovenous phase on a 48-year-old male with cholangiocarcinoma. MS-I image depicts the margins and the extent of the hypovascular mass toward the porta more clearly, as compared to the SECT-equivalent and high-kVp image, by enhancing the contrast of the hepatic parenchyma

are indeterminate or considered too small to be characterized on CT, MR is used as a problem-solving tool. DECT datasets can add value for the characterization of such liver lesions and thus can lead to decreased need for additional and more expensive investigations. Spectral curves generated from VME data or quantitative parameters derived from MS-I images can be used as problem-solving tools when small, atypical, or indeterminate lesions are detected incidentally or in an oncological setting.

In a series of 121 patients with focal liver lesions, Wang et al. [29] found that spectral attenuation curves plotted from portovenous phase of DECT can potentially differentiate benign and malignant masses with diagnostic specificities of 100% for hemangioma and cyst (Fig. 5). Lesional iodine concentration measurements between arterial and portovenous phases can also diagnose (Fig. 6) and distinguish HCC from hemangioma [30], focal nodular hyperplasia [31], or hepatic angiomyolipoma [32] and necrotic HCC from hepatic abscesses [33].

In the setting of surveillance for cirrhosis, characterization of atypical lesions is especially important. Although MRI is the traditional modality of choice for such lesions, it may not be widely available and has higher costs. Using ssDECT, Laroia et al. analyzed 37 indeterminate lesions in cirrhotic patients and found that iodine density $\geq$29.5 mg/dl can diagnose HCC with 90.5% sensitivity and 81.2% specificity [22•].

Iodine concentration measurements can also distinguish between malignant (Fig. 7) and benign portal vein thrombus (refer Fig. 6) with high sensitivity and specificity [34].

Assessment of Therapeutic Efficacy

Traditionally size-based tumor response criteria are used for evaluating treatment responses. However, in 2008 Choi et al. proposed improving the assessment of gastrointestinal stromal tumors on antiangiogenic therapy by evaluating change in CT tumor density in conjunction with size [35]. Apfaltrer et al. concluded that the assessment of change in iodine concentration of these lesions may be a more robust parameter than Choi criteria [36]. This was followed by a study from the same group, which found that iodine uptake from DECT also served as a valid prognostic tool for predicting survival in patients with gastrointestinal tumors [37•].

Table 3 Review of literature, published in the last 7 years, on the capability of DECT in assessing conspicuity of focal hyper- and hypovascular hepatic masses

Authors	Years	*n*	Diagnosis	Scanner type	Results
Hypervascular lesion with DECT in arterial phase					
Marin et al. [14]	2009	31	HCC and metastasis from renal cell carcinoma, neuroendocrine tumor and breast	ssDECT (fast kV switching)	80 kVp improved conspicuity of malignant hypervascular hepatic lesions as compared to 140 kVp
Altenbernd et al. [15]	2011	40	HCC	dsDECT (first generation)	80-kVp images more sensitive in lesion detection than blended and 140 kVp
Shuman et al. [16]	2014	72	HCC	ssDECT (fast kV switching)	50-keV images improved subjective lesion conspicuity with equal detection at 77 keV
Altenbernd et al. [17]	2016	20	Uveal melanoma	dsDECT (first generation)	80-kVp images more sensitive in lesion detection than blended and digital subtraction angiography
Hypovascular lesions with DECT in portovenous phase					
Robinson et al. [18]	2010	11	Metastasis from pancreas, colon, stomach, and esophagus	dsDECT (first generation)	Improved attenuation differences between liver parenchyma and lesion at 80 kVp when compared to 120 kVp
Yamada et al. [19]	2012	90	Metastasis from colorectal region, breast, stomach, lung, pancreas, bile duct, gall bladder, stromal tumor, esophagus, ovary, urinary bladder, testis, uterus, and melanoma	ssDECT (fast kV switching)	High contrast-to-noise ratio for hypovascular metastasis detection at 69–70 keV
Caruso et al. [20]	2017	30	HCC, metastasis, and cysts	dsDECT (third generation)	50-keV images with advanced monoenergetic images show higher diagnostic performance over blended images

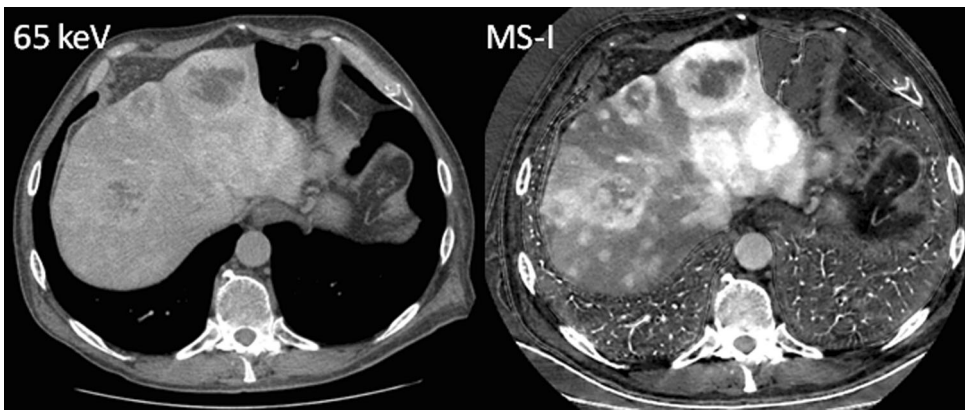

Fig. 3 Visualization of increased number of lesions. ssDECT performed in portovenous phase on a 69-year-old male with pancreatic neuroendocrine tumor. Increased number and improved delineation of the hepatic metastasis is seen on MS-I image

DECT can also be used, subjectively and objectively, to assess the success of different new antiangiogenic therapies in HCC. Color overlay iodine images have been shown to improve reader confidence and decrease interpretation time, during evaluation for recurrent HCC after transcatheter arterial chemoembolization (TACE) [38]. Following TACE, quantification of lipiodol deposition in the tumor by DECT can be potentially used as an indicator to assess drug delivery to the tumor [39]. Measure of iodine uptake has been shown as an optimal tumor response marker after radioembolization as well as sorafenib therapy [40, 41]. The homogeneity and improved CNR of iodine images improves the conspicuity of ablation zone and its margins, which is helpful in the detection of residual or recurrent tumors [42].

While most aforementioned studies evaluated the role of DECT for follow-up, a pilot study has explored its utility in real-time assessment of thermal sensitivity of hepatic tissue

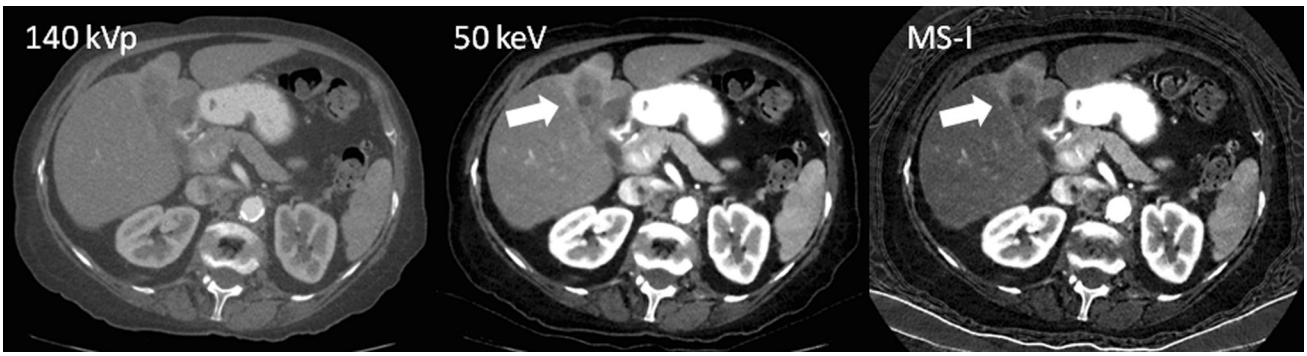

Fig. 4 Improved delineation of lesion enhancement pattern and margins. ssDECT performed in arterial phase on an 84-year-old female with gall bladder cancer. 50-keV and MS-I image shows the heterogeneity of the hypovascular lesion, its extension till the porta hepatis, and the surrounding area of altered perfusion more conspicuously

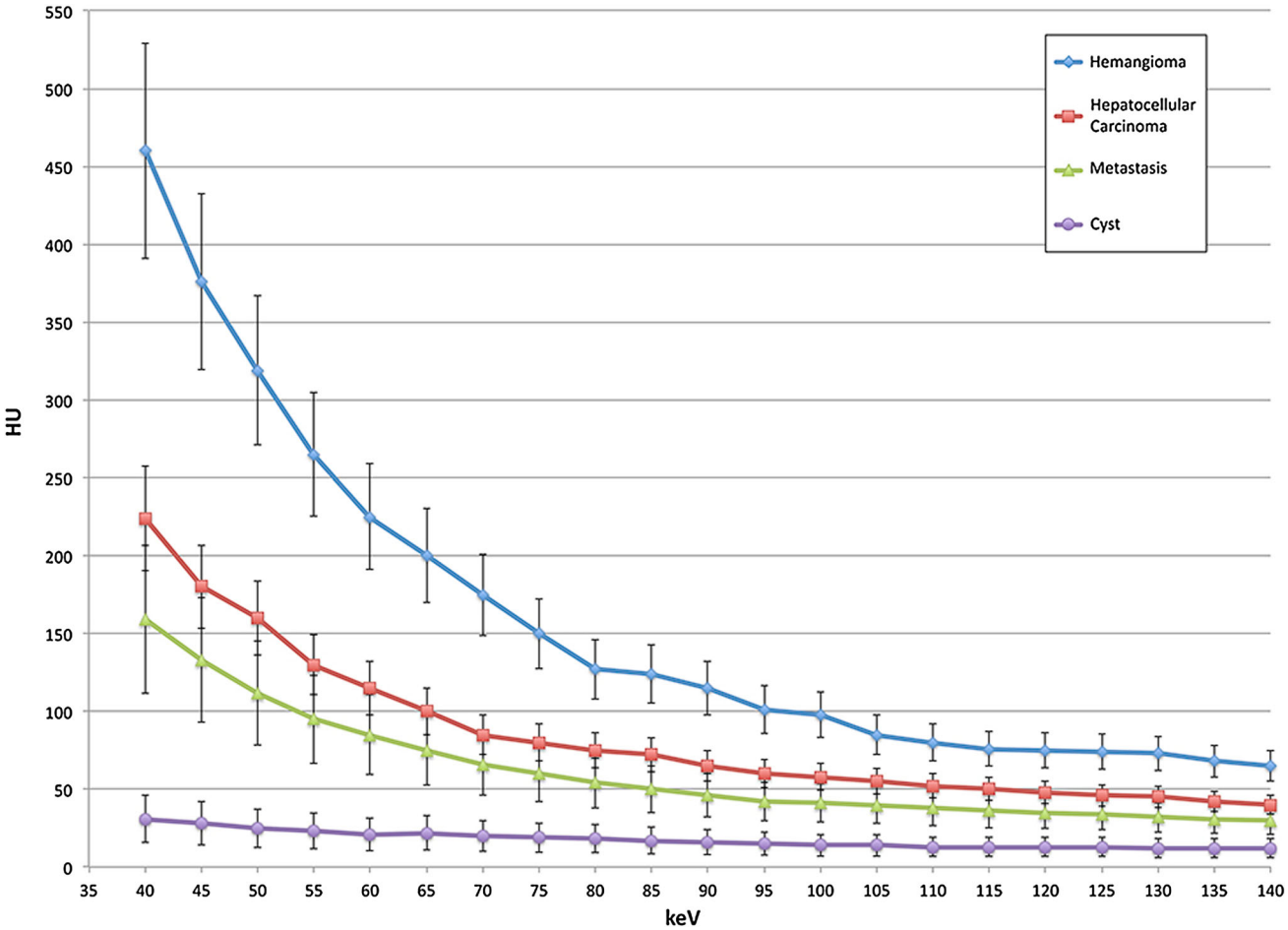

Fig. 5 Spectral curve of hepatic lesions derived from the monochromatic images. The graph depicts attenuation (*Y*-axis) of various lesions at different photon energies (*X*-axis) which aids in mass characterization. *Note* Similar to Wang et al. [29] the highest baseline is seen in hemangioma, followed in order by hepatocellular carcinoma, metastasis, and cyst

during microwave ablation. This has the potential to indicate peri-procedural treatment effectiveness and decrease chances of residual tumors [43].

Besides malignancy, the role of DECT as a functional tool has also been evaluated in infectious hepatic echinococcal disease [44, 45].

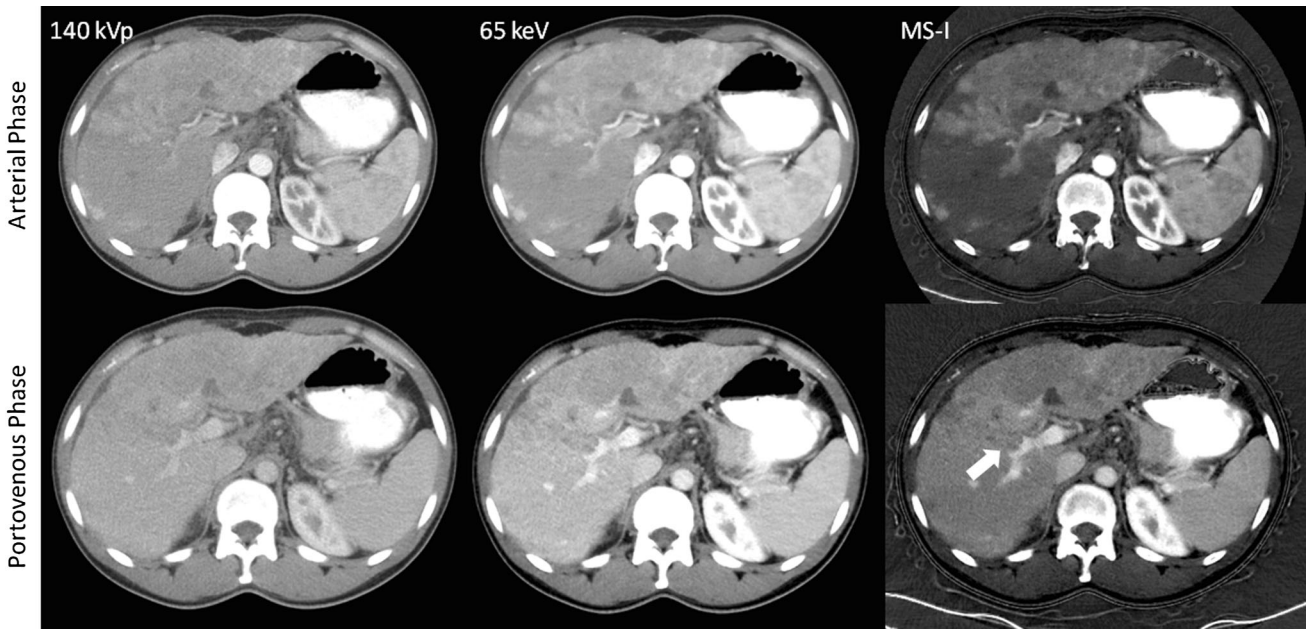

Fig. 6 Dual-phase DECT for delineation of infiltrative mass and tumor thrombus. ssDECT performed in two phases on a 39-year-old male with hepatocellular carcinoma. MS-I image in arterial phase improves the visualization of the hyperenhancing infiltrative lesion in the left lobe. It also increases the conspicuity of other lesions in the right lobe with similar pattern of enhancement. MS-I image of portovenous phase intensifies the contrast between the background parenchyma and lesion, enhancing the visualization of 'wash-out' characteristic of the lesion. *Note* MS-I image also shows enhancing areas within the filling defect in the anterior branch of the right portal vein (*arrow*), confirming the presence of tumor thrombus

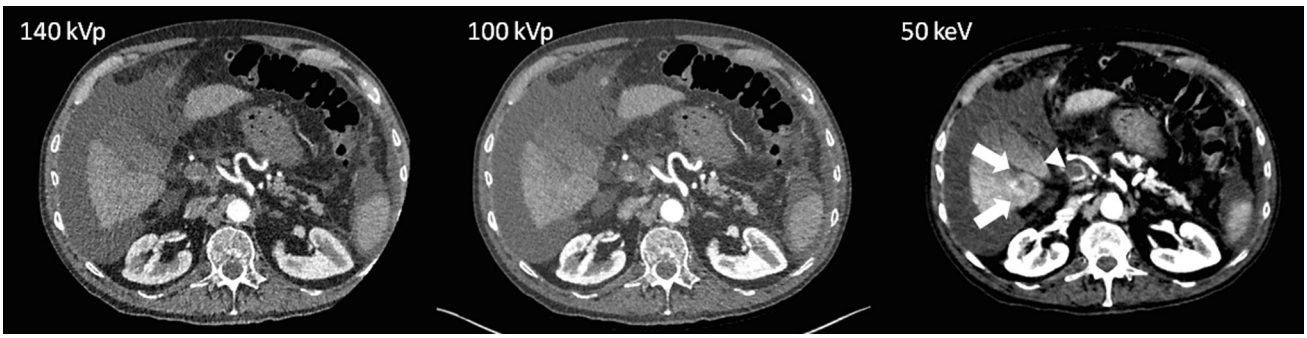

Fig. 7 Thrombus characterization. ssDECT performed in arterial phase on a 68-year-old male with hepatitis C- and alcohol-related cirrhosis. 50-keV image confirms the diagnosis of bland thrombus due to lack of enhancement within the filling defect in superior mesenteric vein (*arrowhead*). Notably, it improves the visualization of a hypervascular lesion (*arrows*; confirmed as hepatocellular carcinoma) in segment VI which would have otherwise been missed

Evaluation of Diffuse Liver Disease: Material Quantification

DECT can quantify materials such as fat, iron, and iodine due to the inherent differences in effective atomic number of these materials from hepatic parenchyma. This forms the basis in diagnosing diffuse liver diseases such as steatosis, hemochromatosis, and fibrosis [46]. Liver biopsy remains the reference standard for diagnosis of diffuse liver disease; however, it is subjected to sampling errors and is invasive. Therefore, different non-invasive imaging modalities are being evaluated as an alternate to histopathology.

Fat

It is important to diagnose the increasingly prevalent fatty liver disease for assessing metabolic status and in liver donors since it is still the reversible stage before progression to fibrosis and cirrhosis [47, 48]. The imaging modalities currently used for assessment have a few limitations. Ultrasound, although easily available, is inaccurate and limited by interobserver variability [49]. Qualitative analysis of SECT images can diagnose moderate–severe steatosis [50]; however, quantitative assessment remains a diagnostic challenge. MR remains the most accurate among

all modalities. However, it is expensive and requires high expertise and special techniques like spectroscopy and patient cooperation for breath-hold [51–54].

Fat shows a decreased attenuation at lower energy levels. Therefore, the spectral curve for hepatic steatosis shows an increase in the attenuation of fat with an increase in tube potential. DECT has been evaluated for hepatic steatosis since late 1900s in phantom studies, animal models, and patient population with mixed results [55–58]. One of the first few successful studies [57] evaluating DECT for quantification found that attenuation change of >10 Hounsfield unit (HU) between 80 and 140 kVp was suggestive of >25% fatty infiltration. Table 4 provides an overview of recent in vivo studies investigating DECT for hepatic fat quantification [5, 59, 60, 61•, 62].

Most of the in vivo studies quantifying fat have been performed on unenhanced phase. For fatty liver, Patel et al. evaluated the feasibility of using contrast-enhanced ssDECT acquisition by comparing it with liver attenuation index from unenhanced SECT [63]. Although they found that threshold concentration 1027 mg/ml from base pair (fat–iodine) MS images can detect fatty liver, no correlation was found on regression analysis to estimate the amount of infiltration. Hyodo et al. calculated the fat volume fraction analysis from multi-material decomposition images and demonstrated the feasibility to stratify fatty liver on true-unenhanced and contrast-enhanced phases [61•].

Iron

Iron overload in the liver is the histological hallmark of hereditary hemochromatosis and transfusion-related hemosiderosis. Iron overload can cause liver damage, eventually leading to the development of cirrhosis, liver failure, and hepatocellular carcinoma. Quantification of liver iron content is necessary to stage and monitor these conditions. Current gold standard for iron quantification is atomic absorption spectrophotometry of non-targeted percutaneous liver biopsy specimens [64]. Table 4 also shows an overview of in vivo studies published in the past 4 years with promising results for iron quantification at clinically significant levels of >10%.

However, MR-based quantification methods are more accurate and, without ionizing radiation, therefore remains the non-invasive marker of choice.

Fat and Iron

The limited success of DECT for fat quantification has been attributed to the spectral overlap between the two energies and simultaneous presence of high-attenuation materials such as iron and iodine. Iron and iodinated contrast media have an inverse effect to fat on DECT attenuation and confound measurements by increasing attenuation with higher iron and/or iodine concentrations [65]. Iron often coexists with fatty liver conditions and chronic liver disease [66]. The introduction of tin filter and development of multi-material dual-energy algorithms have improved the spectral separation and material detection capabilities of DECT [67]. With these advancements, the feasibility to quantify fat in the presence of confounding elements have been shown in ex vivo and animal models [68, 69].

The method for quantification of fat and iron still needs large-cohort clinical validation and no consensus on a single dual-energy index as a marker has yet been established.

Iodine

Invasive liver biopsy is the reference standard for grading of liver fibrosis and cirrhosis. Cirrhosis and fibrosis result in altered liver vasculature due to vasoregulatory imbalances and sinusoidal remodeling [70]. It is proposed that these changes may impact hepatic iodine content which can be potentially detected by DECT.

Recently, DECT has been evaluated for diagnosing cirrhosis and fibrosis. A preliminary study involving 38 cirrhotic patients and 43 healthy patients showed that a combination of measure of iodine concentration normalized to aorta and ratio of concentration in arterial and portovenous phases has the potential to diagnose and stratify grade of cirrhosis [71].

Lamb et al. showed good and reproducible correlation between MR elastography and multi-material decomposition algorithm from DECT to quantify fibrosis [72].

However, further studies with a larger patient cohort and different DECT technologies are needed to validate these findings.

Radiation Dose Reduction

Besides the abovementioned advantages of DECT for disease evaluation, a significant benefit of this technology is series reduction. This stems from the ability of retrospective reconstruction of VUE images from contrast-enhanced acquisition and can be beneficial in reducing radiation dose by up to 30% [36, 73].

VUE can also help in identifying materials such as calcification, fat, and hemorrhage, which would otherwise be concealed in contrast-enhanced images [73]. This aids in diagnosing multiple conditions such as metastasis from osteosarcoma or mucin-producing gastrointestinal tumors,

Table 4 Recent in vivo studies assessing the ability of DECT to quantify fat (steatosis) and iron (hemochromatosis) in unenhanced phase

Authors, years, *n*	Years	*n*	Reference standards	Comparative modality	Scanner types	DECT quantification methods	Results
Fat							
Zheng et al. [59]	2013	52	Ultrasound, SECT	None	ssDECT (fast kV switching)	Spectral curve analysis and measure of HU and % of pixels measuring <0 HU from an ROI drawn on subtracted image[a]	DECT is a promising method and subtraction images may potentially remove discrepancy due to confounding metal accumulation
Kramer et al. [60]	2017	50	MR spectroscopy	SECT, ultrasound, sheer wave elastography, proton-density fat fraction MR	ssDECT (fast kV switching)	Fat-derived material-specific images	DECT does not improve the accuracy of fat quantification over SECT
Hyodo et al. [61•]	2017	33	Biopsy	MR spectroscopy (single-voxel)	ssDECT (fast kV switching)	% Fat volume fraction from multi-material decomposition image	Quantification of fat using DECT was accurate and reproducible
Iron							
Joe et al. [5]	2012	87^	Pathology	3 T MR (in- and out-of-phase gradient-echo T1 and half-Fourier single-shot turbo spin-echo T2-weighted)	dsDECT (first generation)	ΔHU (HU at 80 kVp − HU at 140 kVp)	Similar diagnostic performance of DECT and MR in clinically important levels of iron accumulation and absence of fat as a confounder. ΔHU of 13.8 provides highly specific threshold to exclude significant iron accumulation
Luo et al. [62]	2015	56*	1.5 T MR (spin-echo-based R2 technique)	Same as reference standard	dsDECT (second generation)	Virtual iron content (automatic three-material decomposition similar to iodine quantification)	Above clinically significant iron levels, diagnostic performance of DECT was similar to MR

MR magnetic resonance imaging

[a] Dual-energy subtracted images generated by subtracting monochromatic image at 75 keV from 50 keV. MR correlate available for 23^ and 34* patients, respectively

adenoma, HCC, or angiomyolipoma and lesions on sorafenib therapy [74]. While VUE images from dsDECT provide HU information, the images processed from earlier generations of fast kV switching ssDECT do not provide attenuation values in HU. The new version of fast kV switching ssDECT, however, is proposed to provide HU values in VUE images.

Despite the advantages, there is no consensus on replacing true-unenhanced images with VUE. Studies by Lee et al. and Zhang et al. demonstrated similar attenuation of ablated and treatment-naive lesions, respectively, on true-unenhanced and VUE [42, 75]. Recently, De Cecco et al. demonstrated high subjective quality of VUE and improved detection of lesions smaller than a centimeter on third-generation dsDECT [76]. However, Apfaltrer et al. only found a moderate correlation of attenuation values on both scans [36]. Lee et al. and De Cecco et al. have also described limitations of VUE in the setting of transarterial chemoembolization with lipiodol and small calcified lesions [42, 76].

Apart from the radiation dose reduction due to elimination of true-unenhanced phase acquisition, DECT by itself does not add to the burden of radiation dose beyond that of conventional SECT.

In a series of 74 patients on imaging surveillance for HCC, intra-individual comparison of 64-slice SECT and 128-slice dsDECT acquisitions revealed comparable image quality and radiation dose for both [77]. In fact, for smaller sized patients, dose–length product and effective dose for DECT were lower than those for SECT. Another study has demonstrated the ability to perform abdominal DECT at similar radiation dose to dose-optimized SECT protocols without affecting image noise [9].

Contrast Dose Reduction

Besides a reduction in radiation dose, DECT angiography has been evaluated for reducing the load of intravenous contrast media and consequently contrast-related risk which is beneficial in patients with renal impairment [78]. An animal study has evaluated the effect of contrast media reduction on the detection of hypo- and hypervascular hepatic lesions [79]. They found that without affecting the CNR the amount of contrast media can be reduced by one-fourth to half for hypo- and hypervascular lesions, respectively.

Challenges

As with any imaging modality, awareness of shortcomings of DECT is necessary before investment in scanner and interpretation of images.

Technical limitations with respect to hardware include limited FOV and reduced spectral separation, depending on scanner type. Furthermore, in obese patients, photon starvation in the low-voltage acquisition causes increased image noise (Fig. 8) and limits interpretation of DECT. Photon starvation is especially prominent in the region of the diaphragm, leading to pseudolesions in DECT at the hepatic dome (Fig. 9). Software challenges include lack of enough studies comparing inter-vendor and inter-scanner variability of attenuation values on VUE and iodine concentration on MS-I.

Managerial limitations include workflow challenges due to increased time needed for image reconstructions, need for larger data storage capacity, high cost of scanners, and lack of reimbursement for DECT applications [80].

Fig. 8 Limitation of DECT in an obese patient. ssDECT performed with 80/140 kVp in a patient weighing 310 lbs shows poor image quality of MS-I

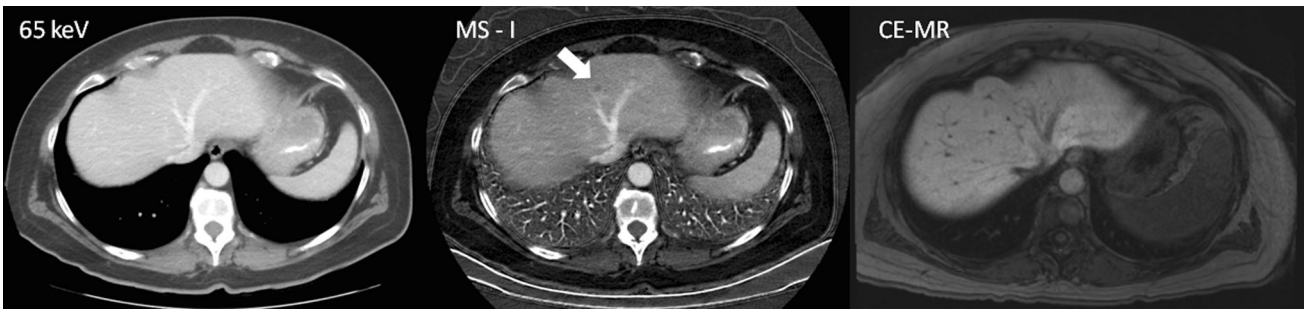

Fig. 9 Pseudolesion on DECT due to photon starvation. ssDECT performed in a patient on oncologic surveillance for rectal cancer and who had normal prior SECT imaging. DECT shows a suspicious new tiny hypovascular lesion in segment IVa. However, current imaging reference standard *contrast-enhanced magnetic resonance imaging* (CE-MR) with hepatocyte-specific contrast agent, performed 13 days later, showed no lesion in the same location

Conclusion

There has been growing utilization of DECT in various abdominal applications. Its acceptance in clinical routine and role in hepatic imaging are evident by recent guidelines from expert committees such as SCBT-MR and American College of Radiology [3]. Development of multi-material decomposition algorithms, tin filter, and optimal CNR images with contrast of low photon energy and noise of high photon energy has improved the DECT technology since its inception. These innovations have enhanced liver lesion detectability in terms of multiplicity and conspicuity. It also shows great promise in the evaluation of different diffuse hepatic deposition disorders; however, it still needs further validation.

Compliance with Ethical Guidelines

Conflict of interest Anushri Parakh reports personal fees from Bayer Healthcare. Vinit Baliyan declares no potential conflicts of interest. Dushyant V. Sahani reports a grant from GE Healthcare and royalties from Elsevier.

Human and Animal Rights and Informed Consent This article does not contain any studies with human or animal subjects performed by any of the authors.

References

Papers of particular interest, published recently, have been highlighted as:

- • Of importance

1. Morgan DE. Dual-energy CT of the abdomen. Abdom Imaging. 2014;39(1):108–34.
2. Silva AC, Morse BG, Hara AK, Paden RG, Hongo N, Pavlicek W. Dual-energy (spectral) CT: applications in abdominal imaging. Radiogr Rev Publ Radiol Soc N Am. 2011;31(4):1031–46–50.
3. De Cecco CN, Boll DT, Bolus DN, Foley WD, Kaza RK, Morgan DE, et al. White Paper of the Society of Computed Body Tomography and Magnetic Resonance on Dual-Energy CT, Part 4: Abdominal and Pelvic Applications. J Comput Assist Tomogr. 2017;41(1):8–14.
4. • Parakh A, Patino M, Sahani DV. Spectral CT/dual-energy CT. In: Medical radiology. Berlin: Springer; 2017. p. 1–21 (cited 3 April 2017). doi:10.1007/174_2017_28. *Spectral information can be obtained by different techniques and there has been significant evolution of DECT technology since its inception. This has caused increased utilization of this technique in clinical practice.*
5. Joe E, Kim SH, Lee KB, Jang J-J, Lee JY, Lee JM, et al. Feasibility and accuracy of dual-source dual-energy CT for noninvasive determination of hepatic iron accumulation. Radiology. 2012;262(1):126–35.
6. Fink C. Liver imaging. In: Johnson T, Fink C, Schönberg SO, Reiser MF, editors. Dual energy CT in clinical practice. Medical radiology. Berlin: Springer; 2011. p. 145–55 (cited 3 April 2017). doi:10.1007/174_2010_55.
7. Megibow AJ, Sahani D, Kachelrieß M, Pisana F, Kuchenbecker S, Schlemmer H-P. Best practice: implementation and use of abdominal dual-energy CT in routine patient care. Am J Roentgenol. 2012;199(5_Supplement):S71–7.
8. Wu X, Langan DA, Xu D, Benson TM, Pack JD, Schmitz AM, et al. Monochromatic CT image representation via fast switching dual kVp. 2009;725845–725845-9 (cited 3 April 2017). doi:10.1117/12.811698.
9. Uhrig M, Simons D, Kachelrieß M, Pisana F, Kuchenbecker S, Schlemmer H-P. Advanced abdominal imaging with dual energy CT is feasible without increasing radiation dose. Cancer Imaging. 2016;16:15.
10. Graser A, Johnson TRC, Chandarana H, Macari M. Dual energy CT: preliminary observations and potential clinical applications in the abdomen. Eur Radiol. 2009;19(1):13–23.
11. Kaza RK, Platt JF, Cohan RH, Caoili EM, Al-Hawary MM, Wasnik A. Dual-energy CT with single- and dual-source scanners: current applications in evaluating the genitourinary tract. Radiogr Rev Publ Radiol Soc N Am. 2012;32(2):353–69.
12. • Mendonca PRS, Lamb P, Sahani DV. A flexible method for multi-material decomposition of dual-energy CT Images. IEEE Trans Med Imaging 2014;33(1):99–116. *Multimaterial decomposition algorithms enable quantification of different materials and has the potential in assessing different elements in the presence of confounding materials like iodine.*
13. Brown CL, Hartman RP, Dzyubak OP, Takahashi N, Kawashima A, McCollough CH, et al. Dual-energy CT iodine overlay

technique for characterization of renal masses as cyst or solid: a phantom feasibility study. Eur Radiol. 2009;19(5):1289–95.
14. Marin D, Nelson RC, Samei E, Paulson EK, Ho LM, Boll DT, et al. Hypervascular liver tumors: low tube voltage, high tube current multidetector CT during late hepatic arterial phase for detection—initial clinical experience. Radiology. 2009;251(3): 771–9.
15. Altenbernd J, Heusner TA, Ringelstein A, Ladd SC, Forsting M, Antoch G. Dual-energy-CT of hypervascular liver lesions in patients with HCC: investigation of image quality and sensitivity. Eur Radiol. 2011;21(4):738–43.
16. Shuman WP, Green DE, Busey JM, Mitsumori LM, Choi E, Koprowicz KM, et al. Dual-energy liver CT: effect of monochromatic imaging on lesion detection, conspicuity, and contrast-to-noise ratio of hypervascular lesions on late arterial phase. Am J Roentgenol. 2014;203(3):601–6.
17. Altenbernd J, Wetter A, Forsting M, Umutlu L. Dual-energy CT of liver metastases in patients with uveal melanoma. Eur J Radiol Open. 2016;25(3):254–8.
18. Robinson E, Babb J, Chandarana H, Macari M. Dual source dual energy MDCT: comparison of 80 kVp and weighted average 120 kVp data for conspicuity of hypo-vascular liver metastases. Investig Radiol. 2010;45(7):413–8.
19. Yamada Y, Jinzaki M, Tanami Y, Abe T, Kuribayashi S. Virtual monochromatic spectral imaging for the evaluation of hypovascular hepatic metastases: the optimal monochromatic level with fast kilovoltage switching dual-energy computed tomography. Investig Radiol. 2012;47(5):292–8.
20. Caruso D, De Cecco CN, Schoepf UJ, Schaefer AR, Leland PW, Johnson D, et al. Can dual-energy computed tomography improve visualization of hypoenhancing liver lesions in portal venous phase? Assessment of advanced image-based virtual monoenergetic images. Clin Imaging. 2017;41:118–24.
21. ECR Online 2017 (cited 3 April 2017). http://ecronline.myesr.org/ecr2017/index.php?p=recorddetail&rid=97a4c4cc-9a3c-4335-805f-8cf2c8ebf881&t=browsesessions#presentation-2b32aaa2-80ff-4875-a94a-0d27f6bdfbcc.
22. • Laroia ST, Bhadoria AS, Venigalla Y, Chibber GK, Bihari C, Rastogi A, et al. Role of dual energy spectral computed tomography in characterization of hepatocellular carcinoma: initial experience from a tertiary liver care institute. Eur J Radiol Open 2016;3:162–71. *DECT can be used as a subjective and objective tool for predicting hepatocellular carcinoma in cirrhotic patients.*
23. Gao S-Y, Zhang X-P, Cui Y, Sun Y-S, Tang L, Li X-T, et al. Fused monochromatic imaging acquired by single source dual energy CT in hepatocellular carcinoma during arterial phase: an initial experience. Chin J Cancer Res. 2014;26(4):437–43.
24. • Husarik DB, Gordic S, Desbiolles L, Krauss B, Leschka S, Wildermuth S, et al. Advanced virtual monoenergetic computed tomography of hyperattenuating and hypoattenuating liver lesions: ex vivo and patient experience in various body sizes. Investig Radiol. 2015;50(10):695–702. *Advanced post processing algorithms are capable of providing images with CNR of low photon energy while retaining image quality of conventional CT. This improves lesion conspicuity.*
25. Marin D, Ramirez-Giraldo JC, Gupta S, Fu W, Stinnett SS, Mileto A, et al. Effect of a noise-optimized second-generation monoenergetic algorithm on image noise and conspicuity of hypervascular liver tumors: an in vitro and in vivo study. Am J Roentgenol. 2016;206(6):1222–32.
26. Mileto A, Nelson RC, Samei E, Choudhury KR, Jaffe TA, Wilson JM, et al. Dual-energy MDCT in hypervascular liver tumors: effect of body size on selection of the optimal monochromatic energy level. Am J Roentgenol. 2014;203(6):1257–64.
27. Schabel C, Bongers M, Sedlmair M, Korn A, Grosse U, Mangold S, et al. Assessment of the hepatic veins in poor contrast conditions using dual energy CT: evaluation of a novel monoenergetic extrapolation software algorithm. RöFo Fortschr Auf Dem Geb Röntgenstrahlen Bildgeb Verfahr. 2014;186(06): 591–7.
28. Su L, Dong J, Sun Q, Liu J, Lv P, Hu L, et al. Spectral CT imaging in patients with Budd-Chiari syndrome: investigation of image quality. Cell Biochem Biophys. 2014;70(2):1043–9.
29. Wang Q, Shi G, Qi X, Fan X, Wang L. Quantitative analysis of the dual-energy CT virtual spectral curve for focal liver lesions characterization. Eur J Radiol. 2014;83(10):1759–64.
30. Lv P, Lin XZ, Li J, Li W, Chen K. Differentiation of small hepatic hemangioma from small hepatocellular carcinoma: recently introduced spectral CT method. Radiology. 2011; 259(3):720–9.
31. Yu Y, Lin X, Chen K, Chai W, Hu S, Tang R, et al. Hepatocellular carcinoma and focal nodular hyperplasia of the liver: differentiation with CT spectral imaging. Eur Radiol. 2013;23(6):1660–8.
32. Yu Y, He N, Sun K, Lin X, Yan F, Chen K. Differentiating hepatocellular carcinoma from angiomyolipoma of the liver with CT spectral imaging: a preliminary study. Clin Radiol. 2013;68(9):e491–7.
33. Yu Y, Guo L, Hu C, Chen K. Spectral CT imaging in the differential diagnosis of necrotic hepatocellular carcinoma and hepatic abscess. Clin Radiol. 2014;69(12):e517–24.
34. Qian LJ, Zhu J, Zhuang ZG, Xia Q, Cheng YF, Li JY, et al. Differentiation of neoplastic from bland macroscopic portal vein thrombi using dual-energy spectral CT imaging: a pilot study. Eur Radiol. 2012;22(10):2178–85.
35. Choi H. Response evaluation of gastrointestinal stromal tumors. Oncologist. 2008;13(Suppl 2):4–7.
36. Apfaltrer P, Meyer M, Meier C, Henzler T, Barraza JM, Dinter DJ, et al. Contrast-enhanced dual-energy CT of gastrointestinal stromal tumors: Is iodine-related attenuation a potential indicator of tumor response? Investig Radiol. 2012;47(1):65–70.
37. • Meyer M, Hohenberger P, Apfaltrer P, Henzler T, Dinter DJ, Schoenberg SO, et al. CT-based response assessment of advanced gastrointestinal stromal tumor: dual energy CT provides a more predictive imaging biomarker of clinical benefit than RECIST or Choi criteria. Eur J Radiol. 2013;82(6):923–8. *Newer drugs affect tumor density rather than size. Therefore size-based guidelines are less accurate than density or iodine-related attenuation measurements in assessing therapeutic response.*
38. Lee J-A, Jeong WK, Kim Y, Song S-Y, Kim J, Heo JN, et al. Dual-energy CT to detect recurrent HCC after TACE: initial experience of color-coded iodine CT imaging. Eur J Radiol. 2013;82(4):569–76.
39. Liu Y-S, Chuang M-T, Tsai Y-S, Tsai H-M, Lin X-Z. Nitroglycerine use in transcatheter arterial (chemo)embolization in patients with hepatocellular carcinoma and dual-energy CT assessment of Lipiodol retention. Eur Radiol. 2012;22(10): 2193–200.
40. Altenbernd J, Wetter A, Forsting M, Umutlu L. Treatment response after radioembolisation in patients with hepatocellular carcinoma—an evaluation with dual energy computed-tomography. Eur J Radiol Open. 2016;25(3):230–5.
41. Dai X, Schlemmer H-P, Schmidt B, Höh K, Xu K, Ganten TM, et al. Quantitative therapy response assessment by volumetric iodine-uptake measurement: initial experience in patients with advanced hepatocellular carcinoma treated with sorafenib. Eur J Radiol. 2013;82(2):327–34.
42. Lee SH, Lee JM, Kim KW, Klotz E, Kim SH, Lee JY, et al. Dual-energy computed tomography to assess tumor response to hepatic radiofrequency ablation: potential diagnostic value of virtual noncontrast images and iodine maps. Investig Radiol. 2011;46(2):77–84.

43. Paul J, Vogl TJ, Chacko A. Dual energy computed tomography thermometry during hepatic microwave ablation in an ex vivo porcine model. Phys Med PM Int J Devoted Appl Phys Med Biol Off J Ital Assoc Biomed Phys AIFB. 2015;31(7):683–91.
44. Jiang Y, Li J, Wang J, Xiao H, Li T, Liu H, et al. Assessment of vascularity in hepatic alveolar echinococcosis: comparison of quantified dual-energy CT with histopathologic parameters. PLoS ONE. 2016;11(2):e0149440.
45. Jiang Y, Wang J, Wang J, Xiao H, Liu W. Clinical application of dual energy spectral CT method in patients with hepatic alveolar echinococcosis. Radiol Infect Dis. 2016;3(3):120–7.
46. Liu X, Yu L, Primak AN, McCollough CH. Quantitative imaging of element composition and mass fraction using dual-energy CT: three-material decomposition. Med Phys. 2009;36(5):1602–9.
47. Enomoto H, Bando Y, Nakamura H, Nishiguchi S, Koga M. Liver fibrosis markers of nonalcoholic steatohepatitis. World J Gastroenterol. 2015;21(24):7427–35.
48. Ma X, Holalkere N-S, Kambadakone RA, Mino-Kenudson M, Hahn PF, Sahani DV. Imaging-based quantification of hepatic fat: methods and clinical applications. Radiogr Rev Publ Radiol Soc N Am. 2009;29(5):1253–77.
49. Bohte AE, Koot BGP, van der Baan-Slootweg OH, van Werven JR, Bipat S, Nederveen AJ, et al. US cannot be used to predict the presence or severity of hepatic steatosis in severely obese adolescents. Radiology. 2012;262(1):327–34.
50. Park SH, Kim PN, Kim KW, Lee SW, Yoon SE, Park SW, et al. Macrovesicular hepatic steatosis in living liver donors: use of CT for quantitative and qualitative assessment. Radiology. 2006;239(1):105–12.
51. Bohte AE, van Werven JR, Bipat S, Stoker J. The diagnostic accuracy of US, CT, MRI and ^{1}H-MRS for the evaluation of hepatic steatosis compared with liver biopsy: a meta-analysis. Eur Radiol. 2011;21(1):87–97.
52. Wu C-H, Ho M-C, Jeng Y-M, Hsu C-Y, Liang P-C, Hu R-H, et al. Quantification of hepatic steatosis: a comparison of the accuracy among multiple magnetic resonance techniques. J Gastroenterol Hepatol. 2014;29(4):807–13.
53. van Werven JR, Marsman HA, Nederveen AJ, Smits NJ, ten Kate FJ, van Gulik TM, et al. Assessment of hepatic steatosis in patients undergoing liver resection: comparison of US, CT, T1-weighted dual-echo MR imaging, and point-resolved ^{1}H MR spectroscopy. Radiology. 2010;256(1):159–68.
54. Lee SS, Park SH, Kim HJ, Kim SY, Kim M-Y, Kim DY, et al. Non-invasive assessment of hepatic steatosis: prospective comparison of the accuracy of imaging examinations. J Hepatol. 2010;52(4):579–85.
55. Mendler MH, Bouillet P, Le Sidaner A, Lavoine E, Labrousse F, Sautereau D, et al. Dual-energy CT in the diagnosis and quantification of fatty liver: limited clinical value in comparison to ultrasound scan and single-energy CT, with special reference to iron overload. J Hepatol. 1998;28(5):785–94.
56. Artz NS, Hines CDG, Brunner ST, Agni RM, Kühn J-P, Roldan-Alzate A, et al. Quantification of hepatic steatosis with dual-energy computed tomography: comparison with tissue reference standards and quantitative magnetic resonance imaging in the ob/ob mouse. Investig Radiol. 2012;47(10):603–10.
57. Raptopoulos V, Karellas A, Bernstein J, Reale FR, Constantinou C, Zawacki JK. Value of dual-energy CT in differentiating focal fatty infiltration of the liver from low-density masses. Am J Roentgenol. 1991;157(4):721–5.
58. Wang B, Gao Z, Zou Q, Li L. Quantitative diagnosis of fatty liver with dual-energy CT. An experimental study in rabbits. Acta Radiol Stockh Swed 1987. 2003;44(1):92–7.
59. Zheng X, Ren Y, Phillips WT, Li M, Song M, Hua Y, et al. Assessment of hepatic fatty infiltration using spectral computed tomography imaging: a pilot study. J Comput Assist Tomogr. 2013;37(2):134–41.
60. Kramer H, Pickhardt PJ, Kliewer MA, Hernando D, Chen G-H, Zagzebski JA, et al. Accuracy of liver fat quantification with advanced CT, MRI, and ultrasound techniques: prospective comparison with MR spectroscopy. Am J Roentgenol. 2017;208(1):92–100.
61. • Hyodo T, Yada N, Hori M, Maenishi O, Lamb P, Sasaki K, et al. Multimaterial decomposition algorithm for the quantification of liver fat content by using fast-kilovolt-peak switching dual-energy CT: clinical evaluation. Radiology 2017;283(1):108–18. *Quantification of iron, using DECT, is feasible in the presence of confounding materials like iron and iodine.*
62. Luo XF, Xie XQ, Cheng S, Yang Y, Yan J, Zhang H, et al. Dual-energy CT for patients suspected of having liver iron overload: Can virtual iron content imaging accurately quantify liver iron content? Radiology. 2015;277(1):95–103.
63. Patel BN, Kumbla RA, Berland LL, Fineberg NS, Morgan DE. Material density hepatic steatosis quantification on intravenous contrast-enhanced rapid kilovolt (peak)-switching single-source dual-energy computed tomography. J Comput Assist Tomogr. 2013;37(6):904–10.
64. Batts KP. Iron overload syndromes and the liver. Mod Pathol Off J U S Can Acad Pathol. 2007;20(Suppl 1):S31–9.
65. Hamer OW, Aguirre DA, Casola G, Lavine JE, Woenckhaus M, Sirlin CB. Fatty liver: imaging patterns and pitfalls. RadioGraphics. 2006;26(6):1637–53.
66. Kohgo Y, Ohtake T, Ikuta K, Suzuki Y, Torimoto Y, Kato J. Dysregulation of systemic iron metabolism in alcoholic liver diseases. J Gastroenterol Hepatol. 2008;23(Suppl 1):S78–81.
67. Thomas C, Krauss B, Ketelsen D, Tsiflikas I, Reimann A, Werner M, et al. Differentiation of urinary calculi with dual energy CT: effect of spectral shaping by high energy tin filtration. Investig Radiol. 2010;45(7):393–8.
68. Ma J, Song Z-Q, Yan F-H. Separation of hepatic iron and fat by dual-source dual-energy computed tomography based on material decomposition: an animal study. PLoS ONE. 2014;9(10):e110964.
69. Fischer MA, Gnannt R, Raptis D, Reiner CS, Clavien P-A, Schmidt B, et al. Quantification of liver fat in the presence of iron and iodine: an ex vivo dual-energy CT study. Investig Radiol. 2011;46(6):351–8.
70. Kim MY, Baik SK, Lee SS. Hemodynamic alterations in cirrhosis and portal hypertension. Korean J Hepatol. 2010;16(4):347–52.
71. Lv P, Lin X, Gao J, Chen K. Spectral CT: preliminary studies in the liver cirrhosis. Korean J Radiol. 2012;13(4):434–42.
72. Lamb P, Sahani DV, Fuentes-Orrego JM, Patino M, Ghosh A, Mendonça PRS. Stratification of patients with liver fibrosis using dual-energy CT. IEEE Trans Med Imaging. 2015;34(3):807–15.
73. Agrawal MD, Pinho DF, Kulkarni NM, Hahn PF, Guimaraes AR, Sahani DV. Oncologic applications of dual-energy CT in the abdomen. Radiogr Rev Publ Radiol Soc N Am. 2014;34(3):589–612.
74. Jakobs TF, Hoffmann RT, Tatsch K, Trumm C, Reiser MF. Therapy response of liver tumors after selective internal radiation therapy. Radiology. 2008;48(9):839–49.
75. Zhang L-J, Peng J, Wu S-Y, Wang ZJ, Wu X-S, Zhou C-S, et al. Liver virtual non-enhanced CT with dual-source, dual-energy CT: a preliminary study. Eur Radiol. 2010;20(9):2257–64.
76. De Cecco CN, Muscogiuri G, Schoepf UJ, Caruso D, Wichmann JL, Cannaò PM, et al. Virtual unenhanced imaging of the liver with third-generation dual-source dual-energy CT and advanced modeled iterative reconstruction. Eur J Radiol. 2016;85(7):1257–64.

77. Purysko AS, Primak AN, Baker ME, Obuchowski NA, Remer EM, John B, et al. Comparison of radiation dose and image quality from single-energy and dual-energy CT examinations in the same patients screened for hepatocellular carcinoma. Clin Radiol. 2014;69(12):e538–44.
78. Fuentes-Orrego JM, Pinho D, Kulkarni NM, Agrawal M, Ghoshhajra BB, Sahani DV. New and evolving concepts in CT for abdominal vascular imaging. Radiogr Rev Publ Radiol Soc N Am. 2014;34(5):1363–84.
79. Chung YE, You JS, Lee H-J, Lim JS, Lee HS, Baek S-E, et al. Possible contrast media reduction with low keV monoenergetic images in the detection of focal liver lesions: a dual-energy CT animal study. PLoS ONE. 2015;10(7):e0133170.
80. Megibow AJ, Chandarana H, Hindman NM. Increasing the precision of CT measurements with dual-energy scanning. Radiology. 2014;272(3):618–21.